1.0

2.8   2.5

3.2   2.2

1.1   2.0

1.8

1.25   1.4   1.6

MICROCOPY RESOLUTION TEST CHART

ADA087011

AFGL-TR- 80-0141 ✓

LEVEL II C 12

MODELLING OF EQUATORIAL PHASE AND AMPLITUDE SCINTILLATIONS FROM
OGO-6 AND AE IRREGULARITY DATA

SANTIMAY BASU
SUNANDA BASU

The Trustees of Emmanuel College
400 The Fenway
Boston, Massachusetts 02115

DTIC
SELECTED
JUL 2 2 1980
C

November 1979

Scientific Report No. 1

Approved for public release; distribution unlimited.

AIR FORCE GEOPHYSICS LABORATORY
AIR FORCE SYSTEMS COMMAND
UNITED STATES AIR FORCE
HANSCOM AFB, MASSACHUSETTS 01731

DDC FILE COPY

80 7 21 003

SECURITY CLASSIFICATION OF THIS PAGE (When Data Entered)

REPORT DOCUMENTATION PAGE		READ INSTRUCTIONS BEFORE COMPLETING FORM
1. REPORT NUMBER AFGL-TR- 80-0141	2. GOVT ACCESSION NO. AD-A087011	3. RECIPIENT'S CATALOG NUMBER
4. TITLE (and Subtitle) Modelling of Equatorial Phase and Amplitude Scintillations from OGO-6 and AE Irregularity Data		5. TYPE OF REPORT & PERIOD COVERED Scientific No. 1, 1 Mar 78-28 Feb 79
		6. PERFORMING ORG. REPORT NUMBER
7. AUTHOR(s) Sunanda Basu Santimay Basu		8. CONTRACT OR GRANT NUMBER(s) F19628-78-C-0005
9. PERFORMING ORGANIZATION NAME AND ADDRESS Emmanuel College 400 The Fenway Boston MA 02115		10. PROGRAM ELEMENT, PROJECT, TASK AREA & WORK UNIT NUMBERS 62101F 4643AAAA
11. CONTROLLING OFFICE NAME AND ADDRESS Air Force Geophysics Laboratory Hanscom AFB MA 01731 PHG Contract Monitor: Herbert E. Whitney		12. REPORT DATE
		13. NUMBER OF PAGES 27
14. MONITORING AGENCY NAME & ADDRESS(if different from Controlling Office)		15. SECURITY CLASS. (of this report) UNCLASSIFIED
		15a. DECLASSIFICATION DOWNGRADING SCHEDULE

16. DISTRIBUTION STATEMENT (of this Report)

A - Approved for public release; distribution unlimited

17. DISTRIBUTION STATEMENT (of the abstract entered in Block 20, if different from Report)

TECH, OTHER

18. SUPPLEMENTARY NOTES

19. KEY WORDS (Continue on reverse side if necessary and identify by block number)

Scintillation Modelling   Power Spectrum   Electron Density
In-situ Measurements   Spread-F   Equatorial Scint.
Ambient Ionization   F-Region irregularities
Atmospheric-Explorer (AE) Satellites

20. ABSTRACT (Continue on reverse side if necessary and identify by block number)

The technique of modelling equatorial phase and amplitude scintillations from in-situ measurements of irregularity amplitude, ambient ionization density and irregularity power spectrum is outlined. The in-situ measurements do not directly provide information on irregularity layer thickness for which radar backscatter observations are utilized. The

DD FORM 1473   EDITION OF 1 NOV 65 IS OBSOLETE   UNCLASSIFIED
1 JAN 73

MIL-STD-847A
31 January 1973

20.

equatorial scintillation models developed from OGO-6 and AE-C in-situ measurements during the two solstices are presented. Considerable differences in the longitude variation of scintillations are predicted during the two solstices. The model estimates are in good agreement with the available ground based phase and amplitude measurements. Problems associated with the use of bottomside spread-F data for transionospheric propagation modelling at VHF/UHF are also discussed.

MODELLING OF EQUATORIAL PHASE AND AMPLITUDE SCINTILLATIONS
FROM OGO-6 AND AE IRREGULARITY DATA

Santimay Basu and Sunanda Basu

Emmanuel College
Boston, MA 02115

ABSTRACT

The technique of modelling equatorial phase and amplitude scintillations from in-situ measurements of irregularity amplitude, ambient ionization density and irregularity power spectrum is outlined. The in-situ measurements do not directly provide information on irregularity layer thickness for which radar backscatter observations are utilized. The equatorial scintillation models developed from OGO-6 and AE-C in-situ measurements during the two solstices are presented. Considerable differences in the longitude variation of scintillations are predicted during the two solstices. The model estimates are in good agreement with the available ground based phase and amplitude measurements. Problems associated with the use of bottomside spread-F data for transionospheric propagation modelling at VHF/UHF are also discussed.

1. INTRODUCTION

F-region irregularities are the cause of intense scintillations (irregular phase and amplitude fluctuations) of signals transmitted through the ionosphere over the frequency range VHF to 1 GHz at high latitudes and VHF to S-band at equatorial latitudes. While the causative mechanisms of these irregularities remain unresolved and continue to be a subject of multi-technique experiments [1-4], their effects are a cause of serious concern to communications engineers. This is because amplitude scintillations can degrade the performance of high data rate satellite communication links while phase scintillations can impair the performance of satellite systems that use synthetic aperture processing to achieve high angular resolution.

3

Ground-based measurements over two decades have established the broad
morphological features of three major scintillation regions, two covering
the auroral ovals and polar caps and a third one approximately centered
on the magnetic equator [5]. That spread-F observations broadly show
similar occurrence maxima have been documented in many studies [6-10].
While undoubtedly both scintillations and spread-F are caused by irregularities
in the F-region, there are definite differences in the occurrence pattern
of each as a function of sunspot cycle, season and longitude. These will
be discussed further in Section 2. Thus the use of bottomside spread-F
data to modify scintillation models at VHF/UHF must be treated with caution.
Furthermore, both scintillation and spread-F measurements are performed
primarily on the ground and thus cannot provide coverage over ocean surfaces.
Clustering of geostationary satellites at preferred longitudes has also
contributed to uneven scintillation coverage.

Satellites carrying out in-situ observations of irregularity parameters
present a viable alternative for mapping the irregularity morphology at both
high and low latitudes. At high latitudes this technique has been used by
Dyson [12] and Sagalyn et al [13] to map irregularity characteristics.
Good agreement was obtained between the scintillation boundary [11] and the
in-situ irregularity boundary. However no attempt has yet been made to
convert the observed irregularity morphology into a high latitude scintillation
model. We are currently developing such a high latitude scintillation model
with Atmospheric Explorer (AE) satellites, AE-C and AE-D in-situ data.
At the equator, Basu et al [14, 15] used in-situ irregularity data obtained
by OGO-6 to map the equatorial irregularity morphology and convert it into
a scintillation model for the December solstice. A pronounced longitude
variation of equatorial scintillations was evident and comparison with
available ground scintillation measurements was very encouraging, indeed.
In Section 3, the principle of utilizing the in-situ technique for
estimating phase and amplitude scintillations is presented. In Section 4
we shall discuss earlier published results obtained with the OGO-6
satellite and present more recent results obtained with the Atmosphere
Explorer satellites. Available ground based scintillation data are used
to compare the model with actual observations. A brief summary is provided
in Section 5.

2. PROBLEMS OF SCINTILLATION MODELLING FROM SPREAD-F

Fremouw and Rino [16] first developed a global model of amplitude scintillations by postulating a model for the irregularity parameters and improving it by comparing the model predictions of scintillations against available ground scintillation observations. While the step was in the right direction, more than 60% of their thirty modelling categories had to remain untested because of a lack of data at that time. In view of the additional data that have been accumulated within the last five years, it is quite possible that the model can be updated by a similar procedure as had been done by Fremouw et al [17]. Singleton [18-20], on the other hand, utilized the existing large data base of spread-F tabulations in an attempt to improve the existing scintillation models without considering the inherent limitations of this technique. In this section we propose to discuss some of these limitations.

It is well known that scintillations are directly related to the rms fluctuations of electron density, ΔN, and the thickness, L, of such irregularity layers [31]. Spread-F, on the other hand, is generally characterized by Δf_o, where f_o is the critical frequency of the F-layer. Since the electron density at the maximum of the F-layer, N, is proportional to f_o^2, the deviation of the electron density from the mean, ΔN, should be proportional to $f_o \Delta f_o$. Thus this latter quantity should be used to compare with scintillation observations. Briggs [21] could thus resolve the conflicting morphologies of spread-F data as observed at Slough, and radio-star scintillation data observed at Cambridge over a solar cycle. As a result of this study Briggs [21] came to the conclusions that the variation of the spread-F index with season and solar cycle reflects mainly the variation of critical frequency with season and solar cycle. Singleton [22] using a different technique, namely estimating f_o and Δf_o from a number of stations at widely separated geomagnetic latitudes, came to the same conclusion. He found that at all latitudes the magnitude of Δf is greatest when critical frequency is lowest. Thus, we find that background conditions dominate the quantitative measure of the spread-F index whereas the scintillation index is not similarly affected. A quantitative relationship between in-situ irregularity measurements and spread-F index at high and middle latitudes was reported in a recent study by Wright et al [23]. They showed that on a statistical basis,

5

the magnitude of $\Delta N/N$ obtained by OGO-6 can be related to $2\Delta f/f$ read from frequency spread ionograms. This is in agreement with the arguments given above. Thus while a general correlation of spread F and scintillations may be expected, one should not expect a detailed agreement such as in diurnal, seasonal and sunspot cycle patterns of these two quantities. Indeed, cases of anticorrelation of seasonal patterns of spread F and scintillation occurrence are observed both at equatorial and high latitudes. For instance, the seasonal spread-F occurrence maximizes at African longitudes during the June solstice [24]. This is in contrast to the minimum of scintillation occurrence observed at Legon, Ghana by Koster [25]. Koster's data was obtained at high elevation angles using Marisat transmissions at 257 MHz and unambiguously shows minimum occurrence of scintillation during the June solstice.

At high latitudes studies conducted by Penndorf [8], Tao [26] and Olesen and Jepsen [27] have all conclusively proved that spread F in all sectors of the northern hemisphere auroral oval show a winter maximum and summer minimum. Scintillations in the North Atlantic sector of the auroral oval, on the other hand, show a consistent summer maximum and winter minimum for data from Narssarssuaq, Greenland [28]. Thus experimenters should be more cautious in inferring that scintillation patterns would be similar to observed spread-F patterns as is often done in the literature.

In the equatorial region a major problem arises because of the nature of the spreading on ionograms. It has been determined that range spreading is associated with intense scintillations at VHF (R.G. Rastogi, private communication, 1978) and strong radar backscatter [29]. Range spreading cannot be characterized by the Δf parameter which is appropriate as an index for frequency spreading. Spread-F tabulations are, however, dominated by cases of frequency spreading thereby making modelling efforts based on published spread-F data open to serious errors.

Another major problem of using spread-F as an ionospheric irregularity index is the great variation of equipment and convention used to measure and classify spread F. This point was discussed at some length by Lyon et al [24], where they pointed out that the 50 percent reduction of spread-F occurrence during the equinoxes in the American zone as compared to the Afro-Indian zone shown in their Figure 1 is due to equipment differences. The fast-sweep high-power ionosondes being used at Huancayo and Chimbote in the American sector were responsible for obtaining better

6

quality ionograms from which f_oF could be read even in the presence of spreading and hence a smaller number of occurrences of spread-F were reported. A careful analysis of the Huancayo and Ibadan (in the African sector) ionograms by the authors themselves showed no significant variation. However, the results of Lyon et al [24] have been used by Singleton [20] to modify the Fremouw-Rino scintillation model leading to a prediction of much lower equinoctial occurrence of scintillations in the American sector as compared to a station in the African sector. This is contrary to scintillation observations as may be noted by comparing Figures 3 and 6 of Aarons [30]. It is thus quite probable that large errors will be introduced into existing scintillation models by modifying them in such a way as to reproduce faithfully tabulated bottomside spread-F occurrence characteristics.

3. THE TECHNIQUE OF MODELLING EQUATORIAL SCINTILLATIONS FROM IN-SITU DATA

A measure of the temporal fluctuations or scintillations of signal phase and amplitude which is recorded by a receiver on the ground is provided by the scintillation index [31]. The normalized second central moment of signal intensity (I) is used to represent the S_4 index of amplitude fluctuations given by

$$S_4^2 = \frac{\overline{I^2} - (\overline{I})^2}{(\overline{I})^2} \qquad (1)$$

On the other hand, the index of temporal phase fluctuations is represented by the variance in phase, σ_ϕ^2.

In the framework of diffraction theory, the indices of phase (σ_ϕ) and amplitude (S_4) fluctuations can be related to the irregularity parameters in the ionosphere. Initially, the above relationship was developed for an assumed gaussian form of irregularities. However, Dyson et al [32] showed by use of in-situ data that the irregularities at F-region heights do have a power law type of irregularity power spectrum with one-dimensional spectral index of 2 corresponding to a 3-dimensional index of 4. For such a 3-dimensional irregularity power spectrum with an outer scale wavenumber, K_o, the variance of phase (σ_ϕ^2) and amplitude scintillation index (S_4) in the case of weak scattering have been obtained [33] as

$$\sigma_{\phi}^2 = \frac{1}{2\pi^2} \cdot (r_e\lambda)^2 \cdot (L\sec\theta) <\Delta N^2> K_oG \, (\tau v_{eff})^2 \qquad (2)$$

$$S_4^2 = 8\pi^2 \cdot (r_e\lambda)^2 \cdot (L\sec\theta) <\Delta N^2> \frac{\lambda z\sec\theta}{4\pi} K_oF \qquad (3)$$

where r_e - the classical electron radius (2.8×10^{-15} m)

         λ - the wavelength of probing radio wave

       z,L - irregularity layer height and thickness, respectively

          - zenith angle at irregularity height

    $<\Delta N^2>$ - mean square electron density deviation

       K_o - outer scale wavenumber

   τ, v_{eff} - detrend interval and effective scan velocity of the propagation path across the irregularities

     G,F - geometrical parameters for anisotropic irregularities

It should be noted that equations (2) and (3) can also be expressed in terms of the strength of turbulence parameter, C_s, where $C_s = 8\pi <\Delta N^2> K_o$.

Equation (3) shows that the S_4 index of scintillation can be modelled if information on electron density deviation, ΔN, and the outer scale wavenumber K_o and irregularity layer thickness are available. The axial ratios pertinent to the three dimensional shape of the irregularities (rod or sheet) enter into the geometrical factors G and F in equations (2) and (3) respectively. The available in-situ data do not provide information on G and F and the shape of the irregularities has to be assumed. The modelling of phase variance in equation (2) is related to two additional parameters v_{eff} and τ as discussed by Rino [33]. The parameter, v_{eff}, depends not only on the relative velocity between the propagation path and the irregularities but for anisotropic irregularities, on the direction of motion with respect to the shortest autocorrelation distance of electron density deviation as well. The detrend interval τ is set by the time interval over which the phase variance is to be computed. Thus v_{eff} and τ are set by the particular system for which the phase modelling is to be done.

The major geophysical parameters involved in the modelling of S_4 and σ_ϕ are thus the rms electron density deviation, ΔN, the form of irregularity power spectrum, the outer-scale wavenumber, K_o, and the irregularity layer thickness, L. Various types of analyzers on board the satellites have been

used to measure the ion concentration (or electron concentration for charge neutrality) at F-region heights [34,13]. Currently, it is possible to sample the ion or electron concentration (N) with an accuracy of .01% with a sampling interval of 4.46 msec corresponding to a spatial resolution of 35 m [35,36]. Such high resolution data from OGO-6 have been used to obtain the irregularity power spectrum which, as already mentioned, indicate that at F-regin heights power-law type of power spectrum prevails.

Supporting evidence has come from the Atmosphere-Explorer (AE) Satellites. Figure 1 shows the irregularity power spectra obtained over a 3-sec time interval close to the F-layer peak near the dip equator by AE-E on March 27-28, 1977 (J.P. McClure, private communication, 1978). The irregularity power spectra obtained both by the FFT technique (indicated by dots) and maximum entropy method (continuous curve) are indicated. The irregularity wavelengths along the abscissa are obtained by converting wavenumbers into wavelengths by utilizing the satellite velocity. The corresponding rms irregularity amplitude $\Delta N/N$ and ambient ionization density are indicated in the caption. Combining the two parameters one obtains $\Delta N = 10^{11}$ m^{-3}. The power spectrum obtained by both techniques is very similar and is observed to follow a power law variation with an index of n = 2. Since the satellite obtained one-dimensional irregularity power spectrum, the spectral index of 3-dimensional irregularity power spectrum is p = n + 2 = 4. Another important aspect of the spectrum is the outer scale dimension. The spectrum, however, does not exhibit any outer scale upto 10 km and therefore near the F peak the outer scale length is greater than 10 km. This type of spectrum forms the basis of model equations (2) and (3).

For the development of a morphological model of scintillations, measurements of irregularity amplitude, $\Delta N/N$, as computed from T sec of data are utilized in conjunction with simultaneous measurement of electron density N. A combination of $\Delta N/N$ and N data provides the required ΔN parameter as a function of position and time. In case the satellite altitude is much lower than the height of maximum ionization, proper allowance should be made in deriving ΔN estimates. The in-situ measurements of irregularity spectrum as shown in Figure 1 and phase scintillation measurements [33] with Wideband satellite indicate that the outer scale at F

9

region heights is large, probably on the order of tens of km. In view of this, the spatial length corresponding to T sec time interval when projected in the direction of shortest correlation distance of electron density deviation sets the apparent outer scale length q_o. The outer scale wavenumber is, therefore, $K_o = 2\pi/q_o$. For the equatorial scintillation model that we developed from the OGO-6 in-situ observations, the time interval was T=5 secs and the outer scale length was considered to be 20 km corresponding to an outer scale wavenumber of $K_o = 0.3$ km^{-1}.

The satellite in-situ measurements pertain to a single altitude and cannot directly provide any information on irregularity layer thickness (1). However, it is possible to obtain estimates of this parameter from in-situ data obtained by satellites in elliptic orbit or direct radar backscatter observations [15,37]. Figure 2 shows the 50 MHz radar backscatter map of F region irregularities acquired by J.P. McClure at Jicamarca (Dip 2°N; Long 76°W) on March 27, 1977. The AE-E measurements shown in Figure 1 pertain to the same night. Such backscatter maps provide information on the range and intensity of backscattered echoes as a function of time. The intensity scale is expressed in dB above a datum level which is 6 dB below the maximum incoherent scatter level. The radar backscatter arises from irregularities with scale lengths equal to half the transmitted wavelength and, therefore, these maps provide information on F-region irregularities with a scale length of 3 m. Two irregularity patches were observed on this night, the first patch being detected between 1945-2045 LT (0045-0145 UT) and the second between 2200-2240 LT (0300-0340 UT). The thickness of the irregularity patches are observed to be in excess of 100 km. A study of a large number of such radar maps indicates that in the equatorial region, a layer thickness of 200 km is a valid assumption for large scale irregularities that give rise to scintillations [38.39,2]. It should be emphasized that the electron density deviation (ΔN) of the irregularities is the single parameter which is most variable and controls scintillations in a sensitive manner. The importance of the in-situ technique stems from the fact that it directly samples the fluctuations of electron density.

4. SCINTILLATION MODEL DEVELOPED FROM IN-SITU DATA

4.1 Equatorial Model during the December Solstice

Based on the OGO-6 in-situ irregularity data obtained during November-December, 1969 and 1970 when the satelliteperigee (400 km altitude) was located over the equatorial region, an occurrence contour of $\Delta N = 10^{10}$ m^{-3} was derived during the early evening hours (1900-2300 MLT) between $\pm 24°$ dip latitudes at all longitudes [14,15]. Considering an outer scale wavenumber $K_O = 0.31$ km^{-1}, equatorial irregularity layer thickness of 200 km and median altitude of 450 km, the above level of ΔN was translated to an amplitude scintillation index of $S_4 = 0.24$ or a peak-to-peak fluctuation of 4.5 dB at 140 MHz for overhead propagation geometry. The percentage occurrence contour of the above level of equatorial scintillation during the D months (November-December) in the early evening hours under sunspot maximum conditions is shown in Figure 3. The pronounced longitude varition of scintillation predicted by this model and its agreement with ground scintillation measurements have been discussed at length in Basu et al [15].

Since we consider that the data length providing ΔN dictates the value of K_O, we may put $v_{eff} \tau = 2\pi/K_O = 20 \times 10^3$ m in equation (2) and derive that for $\Delta N = 10^{10}$ m^{-3} under overhead propagation condition $\sigma_\phi = 2.2$ radians at 140 MHz. For nighttime geostationary satellite observations in the equatorial region, $v_{eff} = 100$ m/sec corresponding to the irregularity drift and therefore, Figure 3 may represent the occurrence contours of $\sigma_\phi \geqslant$ 2.2 radians at 140 MHz with a detrend interval of $\tau = 200$ secs. Since σ_ϕ scales linearly with τ and the radio wavelength, the above statistics are equivalent to $\sigma_\phi \geqslant 0.01$ radian at 1400 MHz with $\tau = 10$ secs. These estimates will also apply to an orbiting satellite if the flight path is aligned parallel to the geomagnetic field when v_{eff} becomes equal to the E-W drift of the irregularities. This is nearly achieved by the Wideband satellite in the Peruvian sector. A limited set of phase scintillation data obtained from the Wideband satellite at Ancon, Peru (kindly made available to us by C.L. Rino of SRI International) during 1977 indicate that the average value of $\sigma_\phi \simeq .05$ radian at 1239 MHz with $\tau = 10$ secs at the magnetic equator for near overhead propagation conditions. This is in fair agreement with our estimates.

11

4.2 Equatorial Model during the June Solstice

The OGO-6 satellite, during its two-year lifetime, did not achieve a suitable perigee-cum-local time combination for equatorial irregularity modelling during the June solstice. Recently, it has been possible to utilize the AE-C in-situ irregularity data for developing an equatorial scintillation model during the J months (June-July). The satellite altitude varied from about 200-600 km over the equatorial region and provided an ideal platform for the study of F region irregularities. Unfortunately, however, the longitude coverage of AE-C satellite was not uniform and only a few orbits were obtained on a specific night. This resulted in a great reduction of the total number of transits available within a specific local time period. Employing a similar technique as outlined in the previous subsection, the percentage occurrence contours of electron density deviation $\Delta N \geqslant 10^{10}$ m^{-3} was obtained within $\pm 24°$ dip latitude at all longitudes in the J months during 1900-2330 MLT under magnetically quiet conditions (Kp = 0-3) and is shown in Figure 4. As discussed before, the above level of $\Delta N = 10^{10}$ m^{-3} corresponds to an amplitude scintillation index of $S_4 = 0.24$ (or a peak-to-peak fluctuation of 4.5 dB) at 140 MHz for overhead propagation conditions which is equivalent to phase scintillations of $\sigma_\phi = 0.1$ radian at 140 MHz with a detrend interval of $\tau = 10$ secs or $\sigma_\phi = 0.01$ radian at 1400 MHz with $\tau = 10$ secs for geostationary satellite observations near the geomagnetic equator.

Figure 4 indicates that there is a drastic reduction of scintillation occurrence in the pre-midnight period during the J months as compared to the occurrence characteristics shown in Figure 3 for the same time interval during the D months, particularly in the African and American sectors. It should, however, be noted that Figures 3 and 4 represent respectively the sunspot maximum and minimum conditions. Figure 5 shows the occurrence statistics of an identical level of scintillation obtained from AE-C in-situ data during the J months but in the near and post-midnight period. The observing period encompassed two magnetic storms but due to paucity of data separation on the basis of magnetic activity levels was not possible. The longitude sectors shown shaded indicate that due to reduced number of transits the statistics over these regions is unreliable.

12

Considering the remaining portions of the diagrams, a general enhancement of scintillation occurrence may be noted at all longitudes.

The occurrence statistics of scintillations during the J months developed from in-situ data and shown in Figures 4 and 5 are in good agreement with ground scintillation observation of Huancayo (courtesy A. Bushby) and Legon (courtesy of J.R. Koster) as shown in Figures 6 and 7. We show in these diagrams the nighttime patterns of scintillation occurrence for the low (Kp = 0-3) and high (Kp = 4-9) magnetic indices observed during the same period at Huancayo, Peru and Legon, Ghana, respectively. Figure 6 shows the statistics of SI > 4 dB obtained at Huancayo during June-July, 1974 from 137 MHz transmissions of ATS-3 whereas Figure 7 shows the statistics of SI > 6 dB observed at Legon from the same satellite. A higher level of scintillation index was chosen for Legon to account for thelower elevation angle of ATS-3 satellite when viewed from this station. Figure 6 indicates that at Huancayo, the occurrence of scintillations is as low as 10% in the pre-midnight period during the J months under magnetically quiet conditions. This is in good agreement with the 15% occurrence near Huancayo derived from in-situ data under quiet periods (Kp = 0-3) and shown in Figure 4. Figure 6 shows that under magnetically active conditions, the occurrence of scintillation is greatly enhanced. The increase of scintillation with magnetic activity in the Huancayo sector during the J months has been documented before [41,30]. As mentioned earlier, the statistics of scintillations obtained from in-situ data during the midnight and post-midnight period for all magnetic conditions (Kp = 0-9) and shown in Figure 5 encompassed two magnetic storms. In fact, all the AE-C transits in this figure that recorded irregularities between -20° and -100° longitudes occurred during disturbed period. The enhanced scintillation in the Huancayo sector predicted by Figure 5 thus corresponds very well with the observational results shown in Figure 6.

Figure 7 shows the behavior of ground scintillation results at Legon during June-July, 1974 and indicates that under magnetically quiet conditions (Kp = 0-3), a scintillation occurrence of about 20% is obtained primarily in the pre-midnight period. Contrary to the usual inverse correlation with magnetic activity [30], Figure 7 shows enhanced scintil-

13

lation occurrence during magnetic activity. The enhancement observed in the
present data set is confined to the pre-midnight hours. This behavior is
somewhat different from that noted in the Huancayo sector (Figure 6) where
enhancement of scintillation occurred during both pre- and post-midnight
periods. The quiettime occurrence of scintillation observed at Legon and
shown in Figure 7 is in agreement with the quiettime statistics obtained
with the in-situ data around Legon (LE) as shown in Figure 4. The be-
havior of scintillations in this sector obtained from in-situ data during
the post-midnight period (Figure 5) could not, however, be compared with
the observational results as the number of AE-C transits over the Legon
sector was very small.

Combining Figures 3, 4, and 5, it may be noted that the occurrence of
scintillations at Kwajalein (KW) is highest in the J-months during the
post-midnight period. This is in agreement with the observations of SRI
International performed at Kwajalein during 1977 [42].

It should, however, be noted that while Figure 3 providing the statis-
tics of scintillation during the D-months was based on 250 transits of
OGO-6 satellite, Figures 4 and 5 providing the occurrence statistics
during the J-months were based on a total of only 105 transits of AE-C
satellite. The estimates should therefore be considered preliminary
and we are currently attempting to enlarge the data base by using data
from AE-E.

5. CONCLUSIONS

The satellite in-situ irregularity measurements provide a direct
measurement of electron density deviation (ΔN) parameter which can be used
to develop models for amplitude and phase scintillations. In view of the
insufficient coverage of ground scintillation observations caused by either
the absence of suitable ground scintillation locations or satellites, the
usefulness of in-situ probing with unlimited latitude and longitude
coverage cannot be overemphasized. The evaluations made in the previous
section show that scintillation models based on the quantitative measure
of electron density deviation (ΔN) by satellite provide realistic esti-
mates. Although, the models that we have developed so far pertain to the

equatorial region, it is be no means limited to this region. Currently, a high latitude scintillation model based on AE-C and AE-D data is being developed.

It should, however, be mentioned that our current efforts are based on satellites whose primary function was not concerned with irregularity measurements at F region heights for scintillation modelling. As such, the constraints imposed on satellite altitude, time of transit, etc., limited our data base. A dedicated satellite performing such measurements at F-region altitudes with suitable orbital characteristics will be an ideal vehicle for the development of a world-wide model of phase and amplitude scintillations.

6. ACKNOWLEDGMENTS

7. REFERENCES

1. J. Aarons, J. Buchau, S. Basu and J.P. McClure, J. Geophys. Res. 83, 1659, 1978.

2. S. Basu and J. Aarons, AFGL Report No. TR-77-0264, Air Force Geophysics Laboratory, Hanscom AFB, MA 01731, 1977.

3. S. Basu and M.C. Kelley, J. Atmos. Terr. Phys. 39, 1229, 1977.

4. S. Basu and M.C. Kelley, Radio Sci. 14(3), 1979.

5. J. Aarons, AFCRL Report No. TR-75-0135, Air Force Cambridge Research Laboratories, Hanscom AFB, MA 01731, 1975.

6. T. Shimazaki, J. Radio Res. Lab. Japan 6, 669, 1959.

7. D.G. Singleton, J. Geophys. Res. 73, 295, 1968.

8. R. Penndorf, J. Geophys. Res. 67, 2289, 1962.

9. J.R. Herman, Rev. Geophys. Space Phys. 4, 255, 1966.

10. H. Chandra and R.G. Rastogi, J. Atmos. Terr. Phys. 32, 439, 1970.

11. J. Aarons and R.S. Allen, J. Geophys. Res. 76, 170, 1971.

12. P.L. Dyson, J. Geophys. Res. 74, 6291, 1969.

13. R.C. Sagalyn, M. Smiddy and M. Ahmed, J. Geophys. Res. 79, 4252, 1974.

14. S. Basu, S. Basu, J.N. Bhar and B.K. Guhathakurta, Space Res. 16, 427, 1976a.

15. S. Basu, S. Basu and B.K. Khan, Radio Sci. 11, 821, 1976b.

16. E.J. Fremouw and C.L. Rino, Radio Sci. 8, 213, 1973.

17. E.J. Fremouw, C.L. Rino, A.R. Hessing and V.E. Hatfield, Report 7, Project 4259, SRI International, Menlo Park, CA 94025, 1977.

18. D.G. Singleton, J. Atmos. Terr. Phys. 37, 1535, 1975.

19. D.G. Singleton, Radio Sci. 12, 107, 1977.

20. D.G. Singleton, in: Solar Terrestrial Prediction Proceedings, NOAA, Boulder, CO, 1979.

21. B.H. Briggs, J. Atmos. Terr. Phys. 26, 1, 1964.

22. D.G. Singleton, Aust. J. Phys. 15, 262, 1962.

23. J.W. Wright, J.P. McClure and W.B. Hanson, J. Geophys. Res. 82, 548, 1977.

24. A.J. Lyon, N.J. Skinner and R.W.H. Wright, J. Atmos. Terr. Phys. 19, 145, 1960.

25. J.R. Koster, Final Scientific Report on Grant No. AFOSR-78-3516, University of Ghana, Legon, Ghana, 1978.

26. K. Tao, J. Radio Res. Lab. 12, 317, 1965.

27. J.K. Olesen and S.B. Jepsen, in: Spread-F and Its Effects upon Radio-wave Propagation and Communications, Technivision, Maidenhead, England, 1966.

28. S. Basu, J. Geophys. Res. 80, 4725, 1975.

29. R.G. Rastogi and R.F. Woodman, J. Atmos. Terr. Phys. 40, 485, 1978.

30. J. Aarons, IEEE Trans. Ant. & Propagat. 25, 729, 1977.

31. B.H. Briggs and I.A. Parkin, J. Atmos. Terr. Phys. 25, 339, 1963.

32. P.L. Dyson, J.P. McClure and W.B. Hanson, J. Geophys. Res. 79, 1497, 1974.

33. C.L. Rino, Radio Sci., 1979 (in press).

34. W.B. Hanson, S. Sanatani, D. Zuccaro and T.W. Flowerday, J. Geophys. Res. 75, 5483, 1970.

35. J.P. McClure and W.B. Hanson, J. Geophys. Res. 78, 7431, 1973.

36. J.P. McClure, W.B. Hanson and J.H. Hoffman, J. Geophys. Res. 82, 2650, 1977.

37. R.F. Woodman and C. LaHoz, J. Geophys. Res. 81, 5447, 1976.

38. S. Basu, J. Aarons, J.P. McClure, C. LaHoz, A. Bushby and R.F. Woodman, J. Atmos. Terr. Phys. 39, 1251, 1977.

39. S. Basu, S. Basu, J. Aarons, J.P. McClure and M.D. Cousins, J. Geophys. Res. 83, 4219, 1978.

40. H.E. Whitney, Report No. AFCRL-TR-74-0004, Air Force Cambridge Research Laboratories, Bedford, MA, 1974.

41. J.P. Mullen, J. Atmos. Terr. Phys. 35, 1187, 1973.

42. C.L. Rino, E.J. Fremouw, R.C. Livingston, M.D. Cousins and B.C. Fair, SRI Report No. DNA 4399F, SRI International, Menlo Park, CA 94025, 1977.

8. FIGURE CAPTIONS

Fig. 1. Power spectrum of total ion concentration data acquired by AE-E
satellite over a 3 sec interval at an altitude of 244 km on March
28, 1977 near the dip equator (dip lat.: 2.56°S, long.: 79.11°W)
at 0029 LT. The dots and solid line represent FFT and MEM spectra
respectively. The rms irregularity amplitude $\Delta N/N = 0.27$ and
ambient ionization density $N = 4.7 \times 10^{11} \ m^{-3}$.

Fig. 2. 50 MHz backscatter power map of F-region irregularities acquired
at Jicamarca, Peru on March 27, 1977.

Fig. 3. Percentage occurrence contours of amplitude scintillation index
$S_4 \geq 0.24$ (SI $\geq$ 4.5 dB) or phase scintillation index $\sigma_\phi \geq 0.1$
radian with a detrend interval of τ = 10 secs at 140 MHz (1900-
2300 MLT, Nov-Dec, 1969 and 1970) obtained from OGO-6 in-situ
irregularity data for overhead geometry.

Fig. 4. Percentage occurrence contours of amplitude scintillation index
$S_4 \geq 0.24$ (SI $\geq$ 4.5 dB) or phase scintillation index $\sigma_\phi \geq 0.1$
radian with a detrend interval of τ = 10 secs at 140 MHz (1900-
2330 MLT, July 11-Aug 4, 1974, magnetically quiet conditions)
obtained from in-situ irregularity measurements by Atmospheric
Explorer-C (AE-C) satellite for overhead geometry.

Fig. 5. Percentage occurrence contours of amplitude scintillations with
$S_4 > 0.24$ (SI > 4.5 dB) or phase scintillations with $\sigma_\phi > 0.1$
radian with a detrend interval of τ = 10 secs at 140 MHz (2330-
0300 MLT, June 20-July 9, 1974, magnetically quiet and disturbed
conditions) obtained from AE-C in-situ data for overhead geometry.

Fig. 6. Variation of the percentage occurrence of scintillations SI > 4 dB
at 137 MHz observed at Huancayo with ATS-3 satellite at 70°
elevation during June-July 1974, for magnetically quiet (Kp $\sim$ 0-3)
and disturbed (Kp $\sim$ 4-9) conditions (data courtesy of Instituto
Geophysico del Peru).

Fig. 7. Variation of the percentage occurrence of scintillation SI > 6 dB

at 137 MHz observed at Legon with ATS-3 satellite at 12° elevation during June-July, 1974, for magnetically quiet (Kp $\sim$ 0-3) and disturbed (Kp $\sim$ 4-9) conditions. In view of the low elevation angle of the satellite, the occurrence diagram for SI > 6 dB in this diagram is compatible with SI > 4 dB in Figure 6 (courtesy of J.R. Koster).

FIG. 1

21

MARCH 27-28, 1977
JICAMARCA
50 MHz BACKSCATTER

42-48dB
30-42dB
18-30dB
6-18dB

FIG. 2

SCINTILLATION ESTIMATE FROM OGO-6 DATA

FIG. 3

23

SCINTILLATION ESTIMATE FROM AE-C DATA

FIG. 4

24

SCINTILLATION ESTIMATE FROM AE-C DATA

GEOGRAPHIC LONGITUDE

DIP LATITUDE
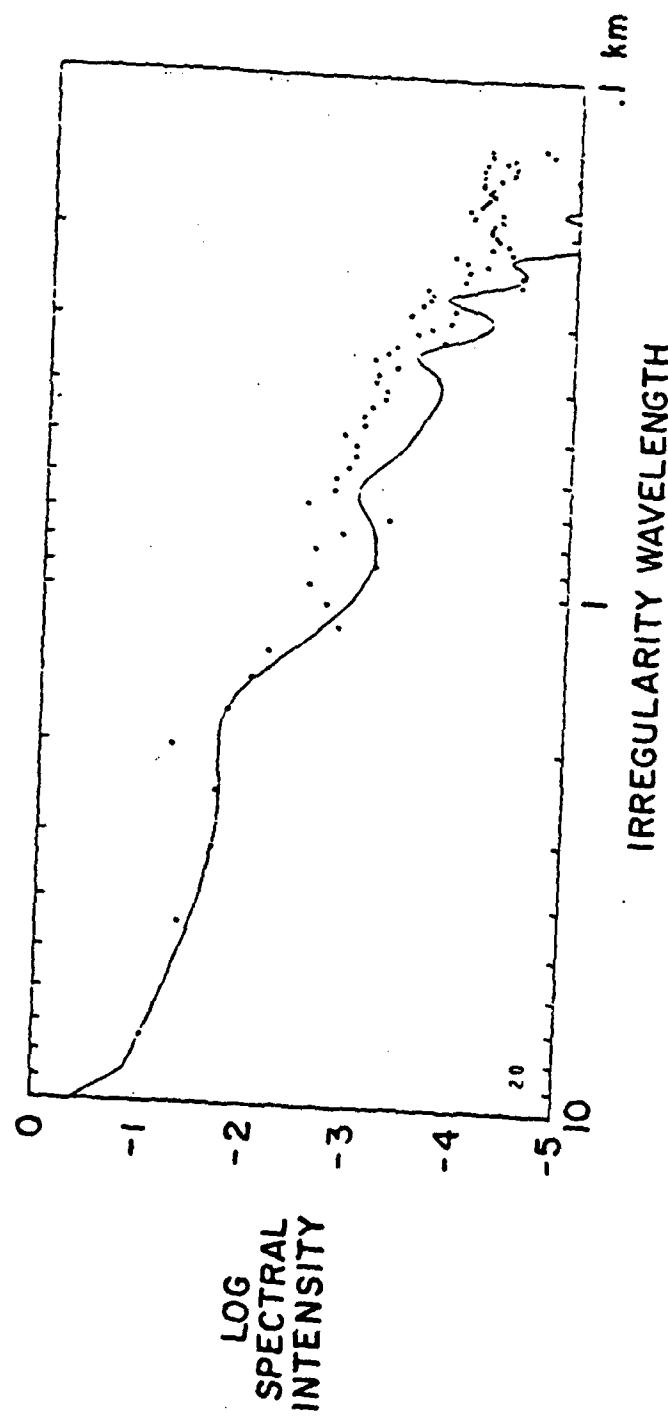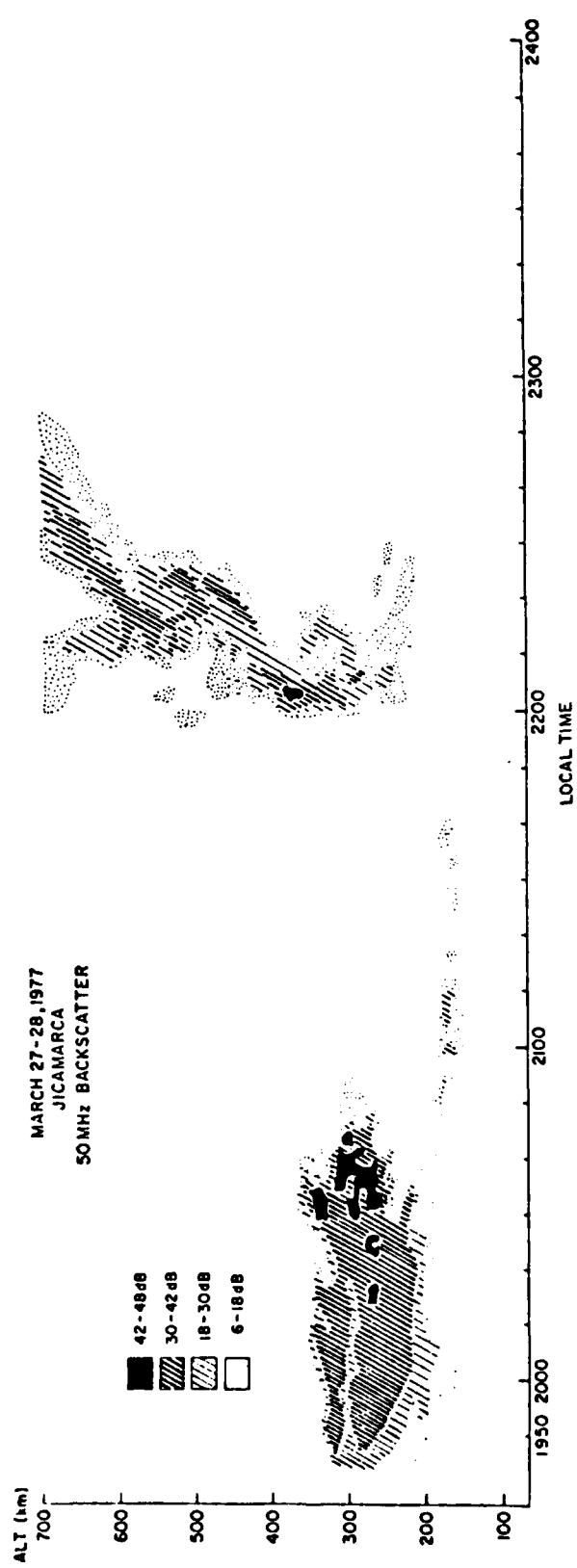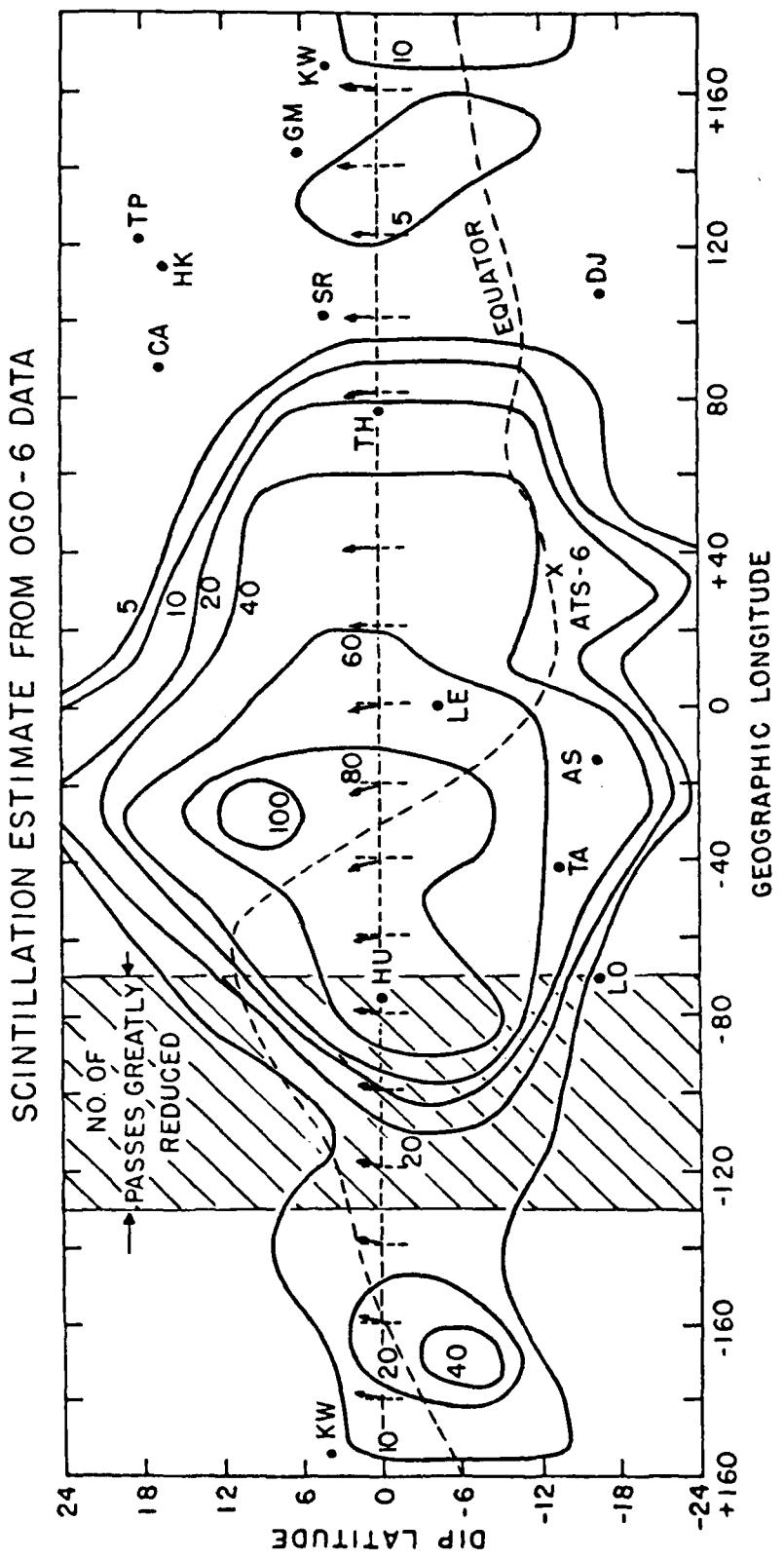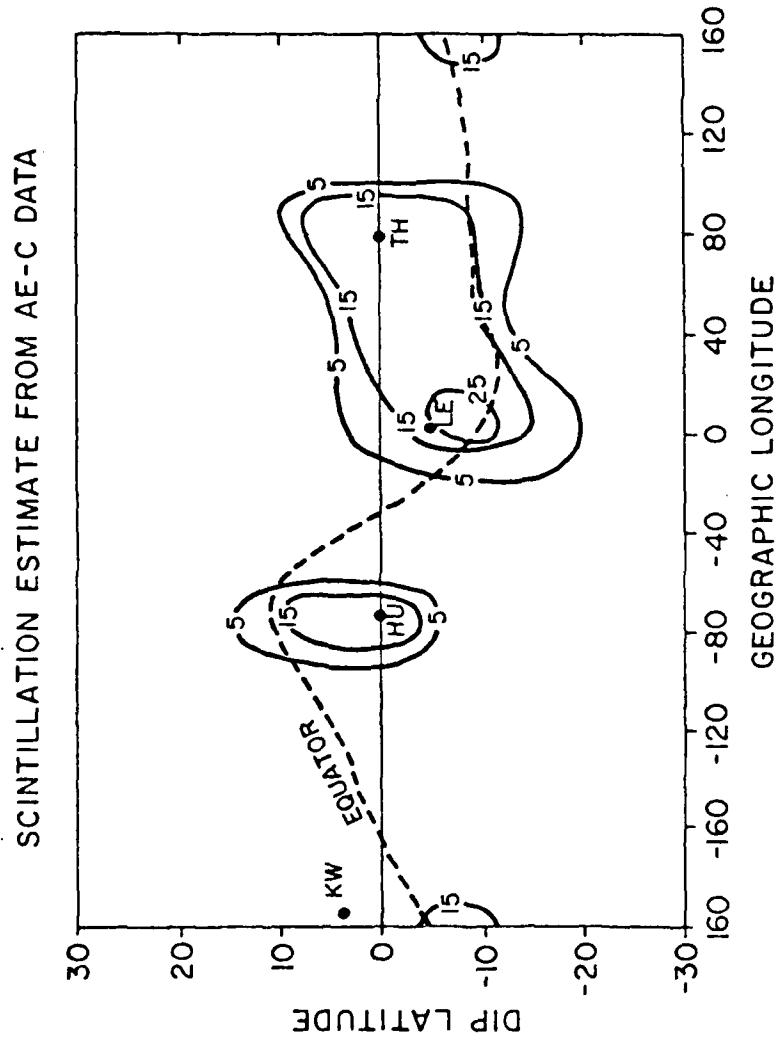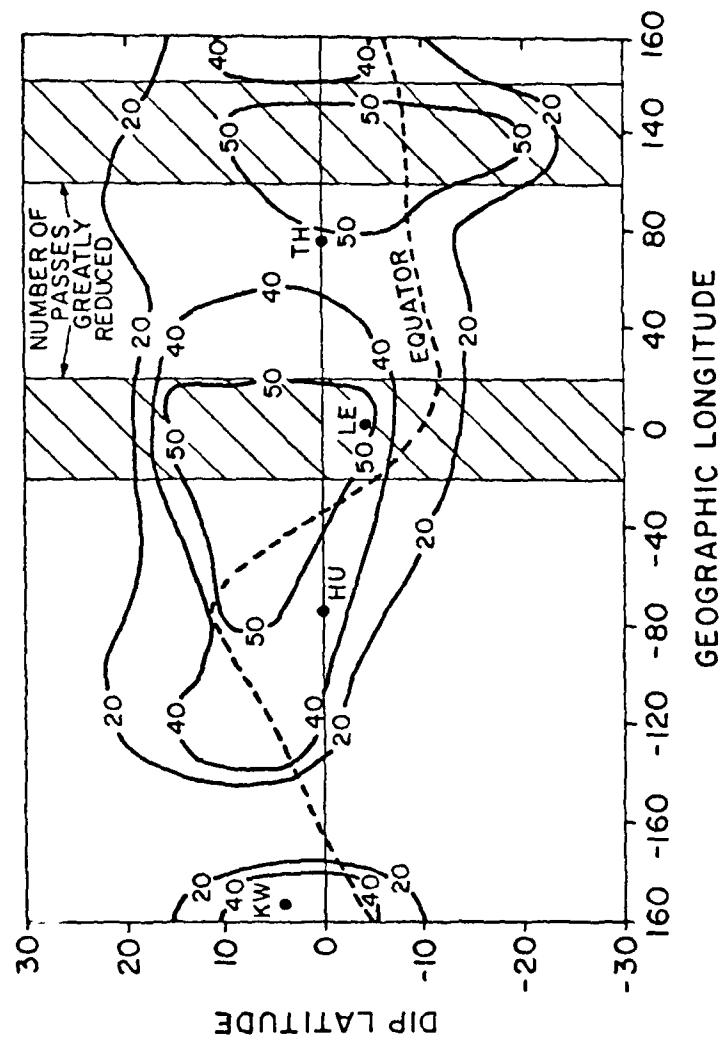
FIG. 5

25

137 MHz A-3 HUANCAYO

JUN/JUL 1974

$K_p = 4-9$

$K_p = 0-3$

PERCENT OCCURRENCE (SI > 4dB)

LOCAL TIME

50 40 30 20 10 0

19 21 23 01 03 05 07
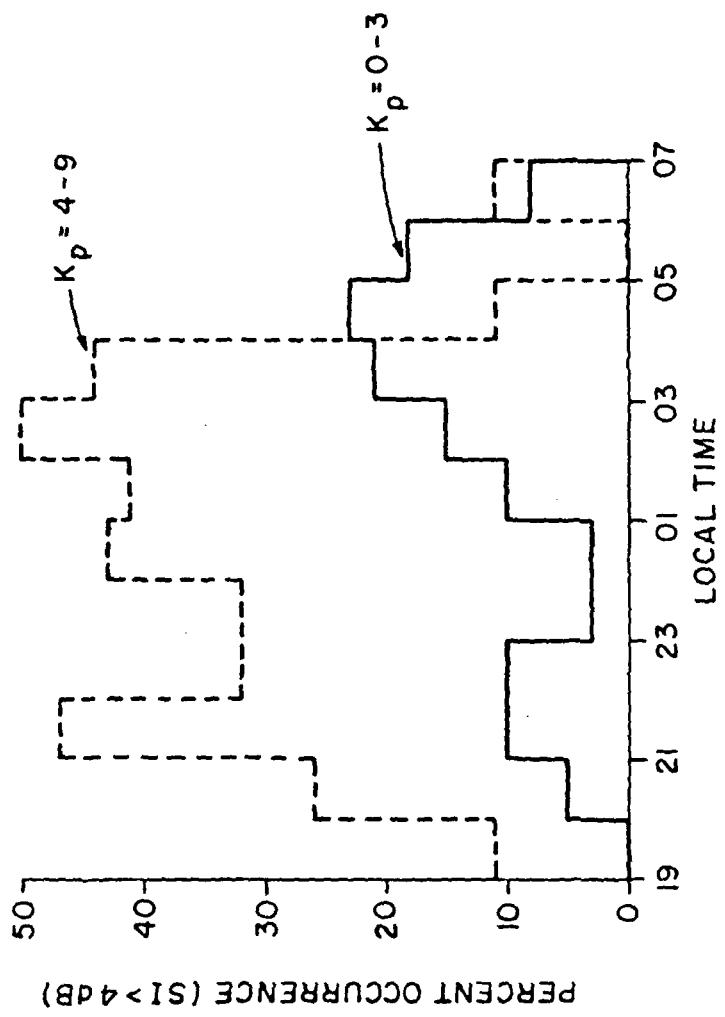
FIG. 6

137MHz A-3 GHANA
JUN/JUL 1974

FIG. 7

27